



Deposited via The University of Sheffield.

White Rose Research Online URL for this paper:

<https://eprints.whiterose.ac.uk/id/eprint/144912/>

Version: Accepted Version

---

**Article:**

Peng, Z., Smith, C. and Stovin, V. (2019) Internal fluctuations in green roof substrate moisture content during storm events: Monitored data and model simulations. *Journal of Hydrology*, 573. pp. 872-884. ISSN: 0022-1694

<https://doi.org/10.1016/j.jhydrol.2019.04.008>

---

Article available under the terms of the CC-BY-NC-ND licence  
(<https://creativecommons.org/licenses/by-nc-nd/4.0/>).

**Reuse**

This article is distributed under the terms of the Creative Commons Attribution-NonCommercial-NoDerivs (CC BY-NC-ND) licence. This licence only allows you to download this work and share it with others as long as you credit the authors, but you can't change the article in any way or use it commercially. More information and the full terms of the licence here: <https://creativecommons.org/licenses/>

**Takedown**

If you consider content in White Rose Research Online to be in breach of UK law, please notify us by emailing [eprints@whiterose.ac.uk](mailto:eprints@whiterose.ac.uk) including the URL of the record and the reason for the withdrawal request.



1 **Internal fluctuations in green roof substrate moisture content during storm events:**

2 **Monitored data and model simulations**

3 Zhangjie Peng\*, Colin Smith and Virginia Stovin

4 Department of Civil and Structural Engineering, The University of Sheffield, Mappin Street,  
5 Sheffield S1 3JD, United Kingdom.

6 \*Corresponding author

7 Email addresses: [zpeng3@sheffield.ac.uk](mailto:zpeng3@sheffield.ac.uk) (Z. Peng), [c.c.smith@sheffield.ac.uk](mailto:c.c.smith@sheffield.ac.uk) (C. Smith).  
8 [v.stovin@sheffield.ac.uk](mailto:v.stovin@sheffield.ac.uk) (V. Stovin).

9 **Keywords:** Green roof; Substrate; Detention modelling; Moisture content; Soil water release  
10 curve (SWRC); Hydraulic conductivity function (HCF).

11 **Abstract**

12 Understanding how the moisture content in a green roof substrate varies during a storm  
13 event is essential for accurately modelling runoff detention. In this paper, a green roof test  
14 bed installed with moisture probes at three depths was used to understand how moisture  
15 content varies during storms. Detailed studies were conducted on five selected storm events.  
16 Physical characterisation tests and field-data based calibrations were performed to acquire  
17 the model parameters. Two alternative detention models, based on Reservoir Routing and  
18 Richard's Equation, were validated against the measured green roof runoff and temporary  
19 moisture storage data. Once the moisture content exceeds local field capacity, its response  
20 at different depths occurs simultaneously during storms, although the recorded data indicate

21 a vertical gradient in the absolute values of local field capacity. Both Reservoir Routing and  
22 Richard's Equation can provide reasonable estimations of the runoff and the vertical moisture  
23 content profiles, although Richard's Equation exhibited stronger vertical water content  
24 gradients than were observed in practise. The vertical water content profile is not sensitive  
25 to the soil water release curve, although the hydraulic conductivity function influences both  
26 the vertical water content profile and runoff rate. The modelled results are highly sensitive to  
27 the bottom boundary condition, with a constant suction head boundary condition providing  
28 a more suitable option than a free drainage boundary condition or a seepage boundary  
29 condition.

## 30 1 Introduction

31 Green roofs can potentially contribute to urban stormwater management through two  
32 processes, the retention of rainfall and the detention of runoff. Green roof hydrological  
33 performance is a function of a combination of physical processes, and these processes are  
34 influenced by the substrate's physical properties. For example, retention performance is  
35 strongly influenced by the water release characteristics, which in turn determine wilting point  
36 and maximum water holding capacity (De-Ville et al., 2017; Fassman and Simcock, 2012; Liu  
37 and Fassman-Beck, 2016). It is widely understood that moisture lost via evapotranspiration  
38 prior to a storm event provides retention capacity within the substrate. It has also been  
39 demonstrated that in a shallow green roof system, losses due to evapotranspiration reduce  
40 when there is restricted moisture available (Poë et al., 2015; Voyde et al., 2010). This  
41 conceptual understanding of retention processes is widely adopted in green roof hydrological  
42 models.

43 However, green roof detention processes are less well understood, and therefore less  
44 consistently represented in green roof hydrological models. It is widely accepted that  
45 detention is of great interest to stormwater engineers and planners. Detention processes  
46 determine the timing and magnitude of peak runoff to the downstream sewer network. The  
47 attenuation and lag of peak runoff may mitigate the risk of localised flooding and reduce the  
48 frequency of combined sewer overflows (CSOs). Many previous studies on green roof  
49 detention have focused on observed performance, using different metrics to characterise  
50 detention from monitored rainfall and runoff data. However, detention performance metrics  
51 – such as Peak Attenuation – can be influenced by many factors, including rainfall  
52 characteristics and antecedent conditions (Stovin et al., 2017). Such metrics do not provide

53 generic modelling capability, in terms of the ability to estimate the temporal runoff profile  
54 associated with an unseen rainfall event applied to an unmonitored green roof.

55 Whilst detention performance metrics are dependent upon external factors such as rainfall  
56 inputs, the underlying detention processes are independent of these factors, and depend only  
57 on the roof's physical configuration (e.g. its slope, substrate characteristics and drainage layer  
58 configuration etc.). Detention performance is dependent upon the substrate's hydraulic  
59 conductivity and porosity, as these properties determine the speed of the water flowing  
60 through the substrate (De-Ville et al., 2017; Liu and Fassman-beck, 2018; Liu and Fassman-  
61 Beck, 2017).

62 Techniques used to model detention include Reservoir Routing (a 'black-box', empirical  
63 approach), a simplified physically-based model in the USEPA's Storm Water Management  
64 Model (SWMM) and unsaturated flow models based on the Richard's Equation. All these  
65 models have demonstrated acceptable levels of accuracy for modelling runoff detention  
66 (Castiglia Feitosa and Wilkinson, 2016; Hilten et al., 2008; Kasmin et al., 2010; Liu and  
67 Fassman-Beck, 2017; Palla et al., 2012; Peng and Stovin, 2017; Soulis et al., 2017).

68 As an example of an empirical approach, Stovin et al. (2015) utilised data from nine  
69 differently-configured green roof test beds to identify suitable Reservoir Routing parameters,  
70 suggesting that the empirically-derived parameter values reflected differences in the basic  
71 configuration (vegetation and substrate components) of individual test beds. However, no  
72 direct links between roof components and detention model parameters were established.

73 The physically-based model, Richard's Equation, potentially has more generic application, as,  
74 unlike the Reservoir Routing model, the parameters depend on measurable physical

75 properties rather than on previously-monitored data. However, Richard's Equation models  
76 depend upon certain models and assumptions about unsaturated flow in soils, that may not  
77 be fully applicable within non-uniform, coarse-grained, heterogeneous green roof substrates.

78 Green roof detention models have typically been validated based on the runoff exiting the  
79 substrate or the whole green roof system (Kasmin et al., 2010; Liu and Fassman-Beck, 2017;  
80 Palla et al., 2009, 2012; Vesuviano et al., 2014; Yio et al., 2013). For example, Liu and Fassman-  
81 Beck (2017) validated the Richard's Equation using measured runoff below a column of green  
82 roof substrate. Hakimdavar et al.(2014) regenerated the runoff profiles of three green roofs  
83 in response to various storms using Richard's Equation. However, in both studies, validation  
84 of the internal vertical water content profile was not reported. Vertical water content profiles  
85 reflect the volume of water temporarily stored in the substrate. As the stored water leaves  
86 the green roof system as runoff, correctly modelling the timing and the volume of temporary  
87 storage is critical to detention modelling. As a physically based model, it is expected that  
88 Richard's Equation should be capable of modelling not only the runoff from the bottom, but  
89 also the dynamic temporary storage within the substrate. However, only a limited number of  
90 studies have investigated green roof detention from the perspective of vertical unsaturated  
91 flows within the substrate. Palla et al. (2009) validated the Richard's Equation (2D form) with  
92 modelled runoff from a full-scale green roof. The modelled vertical water content profile was  
93 compared with measured data at only a few points in time, and the comparisons suggested  
94 that the Richard's Equation tends to underestimate the water content in the substrate. It is  
95 evident that continuous time-series data characterising moisture content variations within  
96 the substrate would provide a valuable addition to the literature on green roof detention.

97 In a full-scale green roof system, detention effects will also include delays due to the runoff  
98 passing through the drainage layer (Stovin et al., 2015). The two-stage green roof detention  
99 model proposed by Vesuviano et al. (2014) took account of the effect of the drainage layer,  
100 with two separate Reservoir Routing models being used to represent detention due to the  
101 substrate and drainage layer respectively. A similar approach was adopted by Palla et al.  
102 (2012), who applied a linear Reservoir Routing model to represent the lateral flow to the  
103 collection barrel. Figure 1 provides a schematic illustration of the conceptual hydrological  
104 model outlined above, indicating the two options for representing substrate detention:  
105 Reservoir Routing and Richard's Equation.

106 **Fig. 1.** Conceptual green roof hydrological model: left – vertical profile through a typical green  
107 roof system indicating the layers associated with retention and detention processes; right –  
108 components of a two-stage detention model, indicating the two alternative options for  
109 representing substrate detention considered in the present paper.

110 The aim of this study is to understand the moisture content dynamics within a green roof  
111 substrate during storm events and to compare field observations with model simulations  
112 made using both a Reservoir Routing model and the Richard's Equation. The aim is achieved  
113 via the following objectives:

- 114 • Experimentally characterise the relevant green roof substrate physical properties;
- 115 • Utilise the moisture content data collected from a green roof test bed to explore  
116 changes in substrate moisture content during storm events;

- 117 • Validate the Reservoir Routing model and the Richard's Equation based on observed  
118 runoff, observed temporarily stored moisture and observed vertical moisture content  
119 profiles (Richard's Equation only);
- 120 • Assess the sensitivity of predictions made with the Richard's Equation to the water  
121 release curve, hydraulic conductivity function and bottom boundary condition.

## 122 **2 Methods**

### 123 **2.1 Experimental set up**

#### 124 **2.1.1 The test beds**

125 The test site, located on a fifth-floor terrace of the Sir Robert Hadfield building (53.3816, -  
126 1.4773), the University of Sheffield, UK, consists of nine green roof test beds (TBs) which vary  
127 systematically in substrate composition and vegetation treatment. The experiment was  
128 established in 2009 and the rainfall-runoff data was collected from April 2010. Each test bed  
129 is 3 m long × 1 m wide with 1.5° slope. The test beds consist of an impermeable hard plastic  
130 tray base, a drainage layer (Zinco Floradrain FD 25-E), a filter sheet (Zinco Systemfilter SF) and  
131 one of nine substrate (80 mm deep) and vegetation combinations. On-site climate data,  
132 including temperature, solar radiation, wind speed and relative humidity, were recorded by a  
133 Campbell Scientific weather station at 1-hour intervals. 0.2 mm resolution AGR-100 tipping  
134 bucket rain gauges manufactured by Environmental Measures Ltd. were used to record the  
135 on-site rainfall. A collection tank equipped with Druck Inc. PDCR 1830 pressure transducer  
136 under each test bed was used for runoff measurement at 1 min intervals. The pressure  
137 transducers were calibrated against volumes on site. A full description of the test beds can be  
138 found in Berretta et al. (2014); De-Ville et al. (2018); and Stovin et al. (2015).

139 Test bed 1 (TB1) is a sedum vegetated green roof with heather and lavender substrate (HLS),  
140 and TB7 is an unvegetated bed with HLS substrate. Both test beds were equipped with  
141 moisture content sensors. The other seven TBs are not relevant to the present study.

142 Substrate moisture content data was collected from March 2011. Three water content  
143 reflectometers (Campbell Scientific CS616), inserted at 20 mm (Top), 40 mm (Mid) and 60 mm  
144 (Bottom) below the surface of the green roof, provide continuous water content  
145 measurement at 5-minute intervals. The rods of the mid and top probes were installed 90°  
146 and 180° respectively from the lower one in order to avoid interference of the measurement  
147 reading taken by the probes. A diagram showing the location of the moisture probes can be  
148 found in Berretta et al. (2014). The water content reflectometers were calibrated at 20°C in a  
149 laboratory environment from 0.05 to 0.40 v/v and an appropriate temperature correction was  
150 applied. The moisture content in the substrate could exceed 0.4 v/v during storms. However,  
151 it is not straightforward to calibrate the moisture probes above 0.4 v/v with our substrates  
152 due to the rapid drainage of water that occurs once the moisture content exceeds field  
153 capacity.

### 154 **2.1.2 Substrate characteristics**

155 The Forschungsgesellschaft Landschaftsentwicklung Landschaftsbau (FLL) (FLL, 2008)  
156 provides the standard guidance for determining green roof substrate physical properties. The  
157 FLL outlines a range of laboratory test methods, apparatus, and standard target values for  
158 substrates to achieve design functions. Properties determined include particle size  
159 distribution, maximum water holding capacity and water permeability (saturated hydraulic  
160 conductivity). Whilst the saturated hydraulic conductivity should provide some indication of  
161 detention behaviour, some questions have been raised about the usefulness of the FLL

162 permeability test. Researchers have reported considerable variation in repeat and replicate  
163 determinations of permeability (Fassman and Simcock, 2012; Stovin et al., 2015).

164 Utilisation of the Richard's Equation requires more fundamental physical properties derived  
165 from soil science, such as the water release curve and the unsaturated hydraulic conductivity  
166 function (Berretta et al., 2014; Liu and Fassman-beck, 2018; Liu and Fassman-Beck, 2017). The  
167 water release curve is a reflection of the substrate's ability to store water (retention and  
168 temporary storage capacity) and the unsaturated hydraulic conductivity is an indicator of the  
169 substrate's water conducting ability (detention performance). As green roof substrates are  
170 not expected to ever reach saturation, the unsaturated hydraulic conductivity characteristics  
171 are more relevant to green roof hydrological modelling than the saturated hydraulic  
172 conductivity (Fassman and Simcock, 2012; Liu and Fassman-Beck, 2018).

173 HLS is a brick-based substrate comprising crushed bricks, pumice and organic matter including  
174 compost with fibre and clay materials. Basic physical properties (bulk density, porosity,  
175 maximum water holding capacity, permeability and particle size distribution) were  
176 determined for the HLS substrate following the FLL guidance (FLL, 2008). To minimise the  
177 uncertainties associated with subsampling, each test was conducted with three replications.

178 The soil water release curve (SWRC) for the HLS substrate was determined by the pressure  
179 plate extraction and hanging column methods. The hanging column method was used to  
180 determine the points on the SWRC at suction heads of 6 cm to 100 cm and the pressure  
181 extractor method was used for high suction heads from 330 cm to 15000 cm. The data points  
182 measured by the pressure extractor method were previously reported by Berretta et al.  
183 (2014) whilst the data points for low suction heads, using the hanging column method, were  
184 newly determined and added to the dataset for model fitting. At high suction heads, the SWRC

185 reflects the difficulty of water extraction from the substrate during dry weather periods; the  
186 water release curve at low suction heads is more relevant to detention processes during  
187 storm events.

## 188 **2.2 Data analysis**

189 The monitored moisture content data spans the period from March 2011 to February 2016.  
190 It was found that 92 out of the 444 identified events had complete and reliable rainfall and  
191 runoff records for TB1 and TB7; these events are referred to as ‘valid’ events. The rainfall-  
192 runoff data collected from 2010 was used to calibrate Reservoir Routing model parameters,  
193 and five representative storm events were selected for model validation. Table 2 lists the  
194 characteristics of the five selected storm events, the performance of TB1 in response to the  
195 storms and the observed initial water content. The monitored rainfall-runoff data for TB7 was  
196 used to derive Reservoir Routing model parameters for the drainage layer and the rainfall-  
197 runoff and moisture content data for TB1 was used to validate the substrate models and  
198 investigate the moisture content behaviour during storms.

199 **Table 2.** Hydrological characteristics of the five selected storm events and TB1 hydrological  
200 performance

## 201 **2.3 Detention modelling**

202 Two approaches are commonly taken to model the detention effect in the substrate: a  
203 lumped (black box) approach based on Reservoir Routing; or a physically-based finite element  
204 approach based on unsaturated flow hydraulics and the Richard’s Equation (e.g. as  
205 implemented in the widely-used HYDRUS-1D model). During a storm event the substrate  
206 moisture content temporarily rises above field capacity, leading to the generation of runoff.

207 In this study, to account for the detention effects in the drainage layer, a two-stage green roof  
 208 detention model, as proposed by Vesuviano et al. (2014) and Palla et al. (2012), was used.  
 209 Two alternative options for modelling the substrate detention were considered here: a  
 210 Reservoir Routing model and the Richards's Equation. A second Reservoir Routing equation  
 211 was used to represent the detention effect in the drainage layer (Fig. 1). The modelled runoff  
 212 and the temporary storage in the substrates were compared with the monitored data to  
 213 evaluate the performance of the models.  $R_t^2$  (Young et al., 1980) was used to describe the  
 214 goodness of fit between modelled and monitored runoff.

## 215 **2.4 Substrate detention models**

### 216 **2.4.1 The Reservoir Routing model**

217 The lumped Reservoir Routing model is given by the following equations:

$$218 \quad Q_{out_t} = kh_{t-1}^n \quad (1)$$

$$219 \quad h_t = h_{t-1} + Q_{in_t}\Delta t - Q_{out_t}\Delta t \quad (2)$$

220 where  $Q_{in}$  is the inflow due to rainfall in mm/min,  $Q_{out}$  is the runoff from the green roof  
 221 substrate in mm/min,  $h$  is the stored water, in mm,  $\Delta t$  is the discretisation time step and  $k$   
 222 ( $\text{mm}^{(1-n)} / \text{min}$ ) and  $n$  (dimensionless) are routing parameters.

### 223 **2.4.2 The Richard's Equation**

224 The 1-D vertical Richard's Equation is given as follows:

$$225 \quad \frac{\partial \theta}{\partial t} = \frac{\partial}{\partial z} [K(h) \left( \frac{\partial h}{\partial z} - 1 \right)] \quad (3)$$

226 where  $\theta$  is volumetric water content,  $K(h)$  is hydraulic conductivity at suction head  $h$  and  $Z$   
 227 is the elevation of the point relative to the reference level. To solve Richard's Equation,

228 functions describing the relationship between volumetric water content and suction head  
 229 (Soil Water Release Curve, SWRC) and the relationship between unsaturated hydraulic  
 230 conductivity and volumetric water content or suction head (Hydraulic Conductivity Function,  
 231 HCF) are needed. For initial investigations, the Durner equation (Durner, 1994) (Eq. 6, 7, and  
 232 8) was used for SWRC, and the Durner-Mualem equation (Eq. 9) was used to estimate  
 233 unsaturated hydraulic conductivity as a function of suction head. Further investigations were  
 234 conducted using the Van-Genuchten model (van Genuchten, 1980) (Eq. 4) for SWRC and the  
 235 Van-Genuchten-Mualem equation (Mualem, 1976) (Eq. 5) for HCF. The Durner equation and  
 236 a new HCF equation (Marshall et al., 1996) (Eq. 10) were also used to investigate the influence  
 237 of the HCF.

$$238 \quad S_e = \frac{\theta - \theta_r}{\theta_s - \theta_r} = [1 + (\alpha h)^n]^{-m} \quad (4)$$

$$239 \quad K(S_e) = K_s S_e^\tau [1 - (1 - S_e^{1/m})^m]^2 \quad (5)$$

$$240 \quad S_e = \frac{\theta - \theta_r}{\theta_s - \theta_r} = w[1 + (\alpha_1 h)^{n_1}]^{-m_1} + (1 - w)[1 + (\alpha_2 h)^{n_2}]^{-m_2} \quad (6)$$

$$241 \quad S_{e1} = [1 + (\alpha_1 h)^{n_1}]^{-m_1} \quad (7)$$

$$242 \quad S_{e2} = [1 + (\alpha_2 h)^{n_2}]^{-m_2} \quad (8)$$

$$243 \quad K(S_e) = K_s (w S_{e1} + (1 - w) S_{e2})^\tau \frac{w \alpha_1 \left\{ 1 - \left( 1 - S_{e1}^{1/m_1} \right)^{m_1} + (1 - w) \alpha_2 \left[ 1 - \left( 1 - S_{e2}^{1/m_2} \right)^{m_2} \right] \right\}^2}{(w \alpha_1 + (1 - w) \alpha_2)^2} \quad (9)$$

$$244 \quad K(\theta) = a \theta^b \quad (10)$$

245 where  $S_e$ ,  $S_{e1}$  or  $S_{e2}$  is the relative saturation,  $\theta$  is volumetric water content,  $\theta_r$  is residual  
 246 water content,  $\theta_s$  is saturated water content,  $h$  is suction head,  $a$ ,  $b$ ,  $\alpha$ ,  $n$ ,  $m$ ,  $w$ ,  $\alpha_1$ ,  $n_1$ ,  $m_1$ ,  
 247  $\alpha_2$ ,  $n_2$ ,  $m_2$  are empirical parameters,  $\alpha$  is the inverse of air-entry value,  $n$  is a pore size

248 distribution index and  $m = 1 - \frac{1}{n}$ ,  $K_S$  is saturated hydraulic conductivity,  $K(S_e)$  is the  
249 unsaturated hydraulic conductivity at  $S_e$ ,  $K(\theta)$  is the unsaturated hydraulic conductivity at  $\theta$   
250 and the tortuosity parameter,  $\tau$  is assumed to be 0.5.

## 251 **2.5 The drainage layer model**

252 For a green roof with a drainage layer, it is expected that detention will occur as the runoff  
253 drains through the drainage layer, and the delay depends on the roof length and drainage  
254 layer configuration (Stovin et al., 2015; Vesuviano et al., 2014; Vesuviano and Stovin, 2013).  
255 Previous studies have confirmed that different types and dimensions of drainage layers may  
256 have different detention characteristics, and a simple nonlinear storage routing model, for  
257 which the parameters only depend on the drainage layer physical characteristics, is capable  
258 of modelling this effect (Vesuviano et al., 2014; Vesuviano and Stovin, 2013; Palla et al., 2012).  
259 In this study, a nonlinear Reservoir Routing equation (Eq. 1 and 2, where  $Q_{in}$  is the inflow to  
260 the drainage layer from the substrate and  $Q_{out}$  is the runoff from the drainage layer) was  
261 applied to model the drainage layer detention.

## 262 **2.6 Model Implementation**

263 As illustrated in Fig. 1, the rainfall-runoff model is characterised by three processes: initial  
264 losses (retention); detention due to the substrate; and detention due to the drainage layer.  
265 As the focus of the present study is on the second process, substrate detention, it was  
266 necessary to eliminate the effects of retention and drainage layer detention from the  
267 monitored rainfall and runoff data.

### 268 **2.6.1 Retention**

269 To model the detention for each selected event, the retention, which was calculated as the  
270 difference between the monitored rainfall and runoff depths, was removed from the start of  
271 the rainfall profile such that only net rainfall was routed to runoff.

### 272 **2.6.2 Reservoir Routing parameters for the drainage layer**

273 The drainage layer is consistent between all test beds. Reservoir Routing parameters for the  
274 drainage layer were identified by eliminating the effects of substrate detention from  
275 monitored runoff responses from TB7. TB7 data is used here for two reasons: firstly, because  
276 its substrate is comparable to one that has been assessed in independent laboratory  
277 detention tests; and secondly because it is an unvegetated system, so no additional detention  
278 effects that might be associated with vegetation or roots are expected.

279 A substrate specific study (Yio et al., 2013) showed that the parameter  $k$  for the substrate  
280 Reservoir Routing model ( $k_g$ ) (subscript  $g$  refers to growing media) relates to the depth and  
281 the permeability of the substrate. The  $k_g$  value is transferable between substrates if they  
282 have similar components, depth and physical properties. The HLS substrate in TB7 has the  
283 same properties as the substrate studied in Yio et al. (2013). Therefore, the TB7 substrate  
284 Reservoir Routing coefficients  $k_g$  and  $n_g$  were assumed to correspond to the values  
285 presented there ( $0.212 \text{ mm}^{(1-n)}/\text{min}$  and 2.0 respectively).

286 The  $k_D$  and  $n_D$  values for the drainage layer were then calibrated from the net rainfall and  
287 runoff data from TB7 by fixing the substrate parameters to  $0.212 \text{ mm}^{(1-n)}/\text{min}$  and 2.0  
288 respectively. Using the TB7 data from the 92 valid storm events, the median calibrated values  
289 of  $k_D$  and  $n_D$  were found to be  $0.026 \text{ mm}^{(1-n)}/\text{min}$  and 1.196 respectively). These parameter

290 values were applied to represent the drainage layer detention in subsequent analyses. The  
291 reservoir routing models were all run at 5-minute time steps.

### 292 **2.6.3 Reservoir Routing parameters for the substrates**

293 As TB1 is a vegetated green roof, even though it shares the same substrate with TB7, the  
294 presence of vegetation could provide extra detention effects, so the substrate Reservoir  
295 Routing parameter ( $k_g$ ) for this test bed needs to be calibrated from monitored rainfall-runoff  
296 data. Calibration was conducted with the net rainfall-runoff data from the 92 valid events by  
297 fixing  $k_D$  to  $0.026 \text{ mm}^{(1-n)}/\text{min}$  and  $n_D$  to 1.196 (the calibrated values from TB7).  $n_g$  was fixed  
298 at a value of 2.0 based on the finding of Yio et al. (2013), who demonstrated that model  
299 performance was insensitive to changes in its value. The calibrated median value of  $k_g$  for  
300 TB1 is  $0.175 \text{ mm}^{(1-n)}/\text{min}$  (Table 1).

301 **Table 1.** Value of parameters used in the Reservoir Routing Model

### 302 **2.6.4 Richard's Equation**

#### 303 **2.6.4.1 SWRC and HCF parameters**

304 To simulate the substrate detention effects using Richard's Equation, the SWRC and HCF  
305 parameters are required. Both the Van-Genuchten model (Eq. 4) and the Durner Equation  
306 (Eq. 6, 7 and 8) were fitted to the data points on the SWRC measured by the hanging column  
307 and pressure plate extractor methods. The fitting and parameter determination were  
308 performed using the SWRC Fit software (Seki, 2010). Initial simulations were conducted with  
309 the Durner Equation and Durner-Mualem Equation (Eq. 9). The saturated hydraulic  
310 conductivity used within the Mualem Equation was determined by the FLL tests ( $K_s = 25$   
311  $\text{mm}/\text{min}$ , Table 4). For further investigations, the Van-Genuchten-Mualem Equation (Eq. 5)

312 and a new HCF (Eq. 10) were also applied to investigate the influence of SWRC and HCF on  
313 the model results.

#### 314 **2.6.4.2 Boundary and initial conditions**

315 For each rainfall event, the upper boundary was set as a Neumann condition in which the  
316 surface flux equals the net rainfall input  $R$  (Eq. 11); the lower boundary was set to be a  
317 constant suction head. The relevant suction head was calculated from the vertically averaged  
318 monitored water content two hours after the rainfall stopped. This value is taken to represent  
319 field capacity (De-Ville et al., 2018; FLL, 2008). The initial condition was set to be a constant  
320 hydraulic head. The moisture content at mid-depth of the substrate was set to the value of  
321 field capacity and the suction head of this middle point was calculated from the SWRC. The  
322 suction heads for the rest of the vertical profile were calculated according to Eq. 12.

$$323 \quad K(h) \left( \frac{\partial h}{\partial z} - 1 \right) = R \quad (11)$$

324 where  $R$  is the net rainfall (cm/min) and all the symbols are as defined before.

$$325 \quad h_i = h_{i+1} - Z_i + 4 \quad (12)$$

326 where  $h_i$  (cm) is the suction head at point  $i$  and  $Z_i$  (cm) is the elevation of point  $i$ . The upper  
327 layer of the substrate was assigned a value of  $i = 1$ . The reference level of elevation (i.e.  $Z =$   
328 0.0 cm) is at the bottom of the substrate, and the value of 4 in Equation 12 represents the  
329 elevation of the middle depth of the substrate.

330 The Richard's Equation was solved in MATLAB using the internal PDE solver by discretising the  
331 80 mm of substrate into 101 node points. The Richard's Equation model was run at 5-minute  
332 time steps. The drainage layer Reservoir Routing model was adopted to model the lateral

333 flows in the drainage layer and generate the runoff from TB1. The parameters for the drainage  
334 layer were the calibrated values as determined before.

### 335 **3 Results**

#### 336 **3.1 Moisture content behaviour during storms**

337 As Table 2 shows, the five selected storms include events in all four seasons. Individual storm  
338 events were defined as being separated by at least 6 hours' continuous dry period (Stovin et  
339 al., 2012). All events had > 8 mm rainfall and generated at least 5 mm runoff. The 21/Oct/2013  
340 event is the heaviest storm with a return period of greater than one year. No rainfall was  
341 retained in the test bed during this storm, which suggests that the test bed was already at  
342 field capacity. In contrast, the 26/Aug/2015 event had a relatively long antecedent dry  
343 weather period (ADWP) and the return period for this event is less than 1 year. In this storm  
344 event, 61% of the rainfall was retained by the green roof test bed.

345 Fig. 2 presents the rainfall, runoff and moisture content data from TB1 for the five selected  
346 rainfall events. Temporary increases in moisture content may be seen to occur in response to  
347 rainfall, after which the monitored moisture content returns to a constant value (assumed  
348 equal to field capacity). The vertical dashed line indicates the time when the first significant  
349 runoff was observed, the dotted line is the time when rainfall stopped, the vertical solid line  
350 is two hours after rainfall stopped and the corresponding measured volumetric moisture  
351 content is interpreted as the local field capacity (Table 3). Any further reduction below field  
352 capacity is expected to be due to evapotranspiration. During the events for which the  
353 substrate initial moisture content was below local field capacity (6/Dec/2012 24/May/2014  
354 and 26/Aug/2015), a significant increase in moisture content was witnessed in the substrate  
355 at the beginning of the storm prior to the onset of runoff. In the event where the substrate

356 was relatively dry (26/Aug/2015) a wetting front ( i.e. a delay in the rise of volumetric water  
357 content at the bottom of the substrate compared with the top) was evident. Once the  
358 substrate moisture content reached local field capacity, it tended to increase simultaneously  
359 with rainfall. The maximum temporary storage in the substrate during the selected storms  
360 was generally less than 0.06 v/v, equivalent to 4.8 mm in an 80 mm deep roof. In general,  
361 runoff was generated after the substrate reached local field capacity, but runoff was  
362 generated before the lower substrate reached its local field capacity in the event on  
363 6/Dec/2012, which may indicate preferential flow.

364 Table 3 lists the local field capacity determined for each event. The three moisture content  
365 probes indicate slightly different moisture content levels at field capacity. Differences in the  
366 absolute values are to be expected in coarse-grained heterogeneous green roof substrates  
367 that may have consolidated over time. The lowest field capacity was found for the event on  
368 25/Aug/2015 and the highest field capacity was associated with the event on 8/Nov/2014,  
369 which is believed to be caused by the seasonal variation of substrate physical characteristics  
370 (De-Ville et al., 2018).

371 **Fig. 2.** Monitored rainfall, runoff and moisture content profiles for the five selected storm  
372 events (vertical dashed line indicates the time significant runoff was firstly observed, dotted  
373 line represents the time rainfall stops, the solid vertical line is the time two hours after rainfall  
374 stops and the corresponding volumetric water content is assumed to indicate local field  
375 capacity).

376

377 **Table 3.** Local field capacity determined for each storm event

### 378 3.2 Substrate characteristics

379 Table 4 lists the results of FLL tests for the HLS green roof substrates. The maximum water  
380 holding capacity determined by the FLL tests is close to the average local field capacity (0.385  
381 vs 0.384), which indicates that the FLL tests do provide reasonable estimations of on-site field  
382 capacity.

383 **Table 4.** HLS Substrate characteristics according to FLL (2008) test methods

384 Fig. 3(a) presents the measured points and fitted water release curves for the HLS substrate.  
385 SWRC A is the fitted Van-Genuchten model and SWRC B is the fitted Durner model. Both  
386 models were fitted using the full experimental dataset, determined by the hanging column  
387 and pressure plate extractor methods. As fig. 3(a) shows, only minor differences were present  
388 between the two models. However, the Durner model has a slightly higher  $R^2$  value (Table 5),  
389 which indicates a better fit to the measured data. This may indicate that the green roof  
390 substrate is more likely to be a dual porosity system (Liu and Fassman-Beck, 2017). Table 5  
391 lists the calibrated parameters for the Van-Genuchten (SWRC A) and Durner (SWRC B)  
392 models. The Fitted Durner parameters (SWRC B) were used in the Richard's Equation to  
393 generate the runoff and vertical water content profile, but further investigation was  
394 conducted with the Van-Genuchten model in the Discussion section.

395 **Table 5.** Fitted parameters for the water release curves for the HLS substrate

396 Application of the Richards' Equation requires data on the substrate's unsaturated hydraulic  
397 conductivity in the form of a Hydraulic Conductivity Function (HCF). Typically, the HCF is  
398 derived from the SWRC via the Mualem model. Figure 3(b) shows the Durner-Mualem (SWRC  
399 B) and Van-Genuchten-Mualem (SWRC A) derived HCFs for the HLS substrate. However,

400 previous authors have questioned the applicability of these derived HCFs to coarse-grained  
401 heterogeneous green roof substrates (e.g. Liu and Fassman-Beck, 2018). Figure 3(b) therefore  
402 includes a third HCF, which has been derived from preliminary laboratory tests (based on the  
403 ASTM steady state infiltration column test method (ASTM, 2015)) undertaken on the HLS  
404 substrate. Given the sparse nature of this preliminary data set, the basic HCF model presented  
405 in Equation 10 has been fitted to the data. Substantial differences may be observed between  
406 the Mualem-based HCF functions and the new function derived from laboratory  
407 measurements. Whilst further work is required to refine the testing procedures and to extend  
408 the laboratory data coverage, it is nonetheless interesting to investigate how the alternative  
409 HCF would affect the model's prediction of substrate runoff detention. The sensitivity of  
410 model predictions to the HCF is therefore considered in the discussion section.

411 **Fig. 3.** Water release curves and hydraulic conductivity functions. (a) SWRC A is fitted by the  
412 Van-Genuchten model, SWRC B is fitted by the Durner model, both models were fitted using  
413 hanging column and pressure plate extractor data; (b) plots of the new HCF and the HCFs  
414 derived from the two SWRC in (a) via the Mualem model.

### 415 **3.3 Model Validation**

416 Fig. 4 compares modelled and monitored runoff from the test bed in response to the five  
417 selected storm events. Note that for both substrate detention models the detention due to  
418 the drainage layer was modelled using the calibrated Reservoir Routing model described in  
419 Section 2.5. With most  $R_t^2$  values higher than 0.6, it is confirmed that both Reservoir Routing  
420 and Richard's Equation can achieve satisfactory results for runoff prediction. Both models give  
421 more accurate predictions of runoff in response to heavy rainfall events. The 21/Oct/2013  
422 (return period >1 year) and the 8/Nov/2014 events (return period nearly 1 year) have the

423 highest  $R_t^2$  values. Both models tend to underestimate the peak runoff and delay the time to  
424 peak runoff slightly for the event on 26/Aug/2015. This may reflect an overestimation of the  
425 detention effect in the drainage layer. Alternatively, the slight difference between the  
426 substrates used in TB7 and Yio et al. (2013) and the introduction of a filter sheet in the field  
427 test beds could result in an overestimation of substrate detention. The two models give  
428 consistent performance. During the heaviest 21/Oct/2013 event, the difference between the  
429 two models is minor. Richard's equation has better performance in the 24/May/2014 and  
430 26/Aug/2015 events when the local field capacity is relatively low compared with the rest of  
431 the events. However, Richard's Equation has worse performance in the 6/Dec/2012 event,  
432 when the local field capacity is high. Except for the fact that the Richard's Equation requires  
433 several input parameters, there is no obvious advantage of the Reservoir Routing model over  
434 the Richard's Equation. The fact that the Reservoir Routing model relies on calibrated  
435 parameters which do not necessarily have physical meaning limits its generic application.

436 **Fig. 4.** Monitored and modelled runoff using the Reservoir Routing model and the Richard's  
437 Equation (Richard's Equation was implemented in MATLAB using SWRC B-Mualem model and  
438 constant suction head lower boundary condition).

439 This type of model validation (based on runoff) has been presented elsewhere. However,  
440 further independent validation is provided by the monitored moisture content data. Fig. 5(a)  
441 shows the dynamic responses of modelled and measured temporary storage in TB1 during  
442 the heaviest 21/Oct/2013 event. The modelled temporary storage curves were smoothed by  
443 performing 4 adjacent points regression. The modelled temporary storage is more dynamic  
444 compared with the measured, which may reflect the response rate of the moisture probes.  
445 However, the overall timing of the temporary storage is modelled well by both models, even

446 though more water is predicted by the Richard's Equation to be stored in the substrate. Whilst  
447 in this case the Richard's Equation appears to overestimate the temporarily stored moisture,  
448 this is not always the case.

449 The temporarily stored runoff, modelled by the Reservoir Routing model, was converted to  
450 volumetric water content using Eq. 13. Fig. 5(b) compares observed versus modelled water  
451 content for all five selected storm events. Both the observed and modelled moisture data  
452 were recorded every 5 minutes, starting from the time when significant runoff was first  
453 observed to the end of the storm. The dotted lines represent  $\pm 5\%$  deviation. The predictions  
454 of both models are consistent, but the Richard's Equation tends to overestimate the water  
455 content in most cases, while the Reservoir Routing model is more likely to underestimate the  
456 water content. Overall, the water content using both models is within  $\pm 5\%$  error.

$$457 \quad \theta_t = \frac{h_t}{80} + \theta_{fc} \quad (13)$$

458 where  $\theta_t$  is the volumetric water content at time  $t$ ,  $h_t$  is the modelled temporary storage by  
459 the Reservoir Routing model (mm),  $80$  is the depth of the substrate (mm),  $\theta_{fc}$  is the depth  
460 averaged local field capacity for each event.

461 As the Richard's equation is solved over a depth profile, validation of the vertical moisture  
462 content profile is possible. Fig. 5(c) compares the modelled and observed moisture content  
463 fluctuations at three depths for the 21/Oct/2013 event. This comparison reveals stronger  
464 vertical gradients in the modelled responses compared with the observed data. Potential  
465 reasons for this are explored within the discussion section.

466 **Fig. 5.** Validation of temporarily stored moisture. (a) depth averaged temporary storage; (b)  
467 scatter plot comparison of water content for all storm events (depth averaged); (c)  
468 comparison of vertical water content profiles.

## 469 **4 Discussion**

470 Modelling of green roof substrate detention using Richard's Equation requires several input  
471 parameters. Conventionally, these parameters are derived from natural soil based empirical  
472 equations. This section aims to investigate the sensitivity of the predictions to the parameters.  
473 The event on 21/Oct/2013 was used to undertake the sensitivity analysis and the influence of  
474 water release curve, hydraulic conductivity function and lower boundary condition were  
475 considered.

### 476 **4.1 Water release curve**

477 The modelling with Richard's Equation reported earlier was based on SWRC B (Fig. 3(a)), in  
478 which a Durner model was fitted to the data points determined by the hanging column and  
479 pressure plate extractor methods. In terms of fitting to measured SWRC data, the differences  
480 between SWRC B (Durner) and SWRC A (Van-Genuchten) are minor. The question raised here  
481 is whether this minor difference in SWRC could influence the overall modelling results. SWRC  
482 A (Fig. 3(a)) was used with the Mualem model to regenerate the runoff and vertical water  
483 content profile for the event on 21/Oct/2013.

484 Fig. 6(a) shows the monitored and modelled runoff using SWRC A-Mualem and SWRC B-  
485 Mualem model. Some noticeable differences are evident between the two models. More  
486 significant detention effects in the substrate were modelled by the SWRC A-Mualem model.  
487 The time to start of runoff was delayed by about an hour, and the model underestimated the

488 peak runoff by nearly 60%. Fig. 6(b) presents the modelled vertical water content profile using  
489 the SWRC A-Mualem model. Compared with Fig. 5(a), in which the vertical water content  
490 profile was modelled using the SWRC B-Mualem model, significantly more water is modelled  
491 to be temporarily stored in the substrate.

492 In terms of SWRC, the two models both have good fits to the measured data and no notable  
493 difference was evident; however, significant differences were observed in the modelled  
494 runoff and vertical water content profile. This appears to be caused by the differences in  
495 SWRC derived HCF. As shown in Fig. 3(b), the HCFs associated with the two models show large  
496 differences. The SWRC A HCF gives lower values of unsaturated hydraulic conductivity than  
497 SWRC B, and as a consequence, more water is predicted to be stored in the substrate. More  
498 discussion on the influence of HCF is provided in section 4.2.

499 **Fig. 6.** Validation of runoff and temporarily stored moisture. (a) monitored and modelled  
500 runoff; (b) monitored and modelled vertical water content profiles using the SWRC A-Mualem  
501 model.

## 502 **4.2 Hydraulic conductivity function**

503 The Mualem equation is not independent of the SWRC; changing the SWRC also changes the  
504 HCF. As shown in Fig. 3(b), SWRC A and SWRC B lead to different estimates of the HCF. As a  
505 consequence, it is difficult to distinguish whether it is the minor difference in SWRC or the  
506 HCF that influences the predictions. In addition, as suggested in previous studies, the Mualem  
507 equation may not provide the best fit to the measured unsaturated hydraulic conductivity  
508 (Liu and Fassman-Beck, 2018). The investigation here aims to assess the influence of HCF on

509 the predictions. The work reported earlier utilized SWRC B in combination with the Mualem  
510 HCF formulation. Here one additional option is considered: SWRC B-Eq. 10.

511 Figure 7(a) shows the modelled runoff using the SWRC B-Eq. 10 formula. Compared with the  
512 runoff modelled by the SWRC B-Mualem model, the peak runoff was reduced by about 70%  
513 compared with the monitored value. Figure 7(b) presents the modelled vertical water content  
514 profile using the Eq. 10 HCF. The maximum water content nearly doubled the quantity shown  
515 in Fig. 5(c). In terms of the runoff prediction and the vertical water content profile, the  
516 Richard's Equation is clearly very sensitive to the HCF, which indicates that a suitable HCF is  
517 needed to correctly characterise the dynamics of water content variation in the substrate.  
518 This observation may be even more relevant when deeper systems (e.g. intensive green roofs  
519 or bio-retention cells) are to be modelled. In this case, despite the fact that Eq. 10 appears to  
520 fit the preliminary laboratory data better than the two other options, SWRC B-Mualem  
521 appears to result in the most representative model prediction.

522 **Fig. 7.** Validation of runoff and temporarily stored moisture. (a) monitored and modelled  
523 runoff; (b) monitored and modelled vertical water content profiles using SWRC B-Eq. 10  
524 model.

### 525 **4.3 Lower boundary condition**

526 Based on the conceptual model outlined in Fig. 1, the Richard's Equation was applied only  
527 when the substrate moisture content was between field capacity and saturation (i.e. to model  
528 the detention). Based on field observations that the water content does not decrease below  
529 field capacity following a storm event, the lower boundary of the Richard's Equation was set  
530 to a constant suction head. However, in some other studies, different approaches have been

531 adopted. For example, Richard's Equation was used to model the retention and detention and  
532 the lower boundary was set to be free drainage in the studies of Liu and Fassman-Beck, (2017)  
533 and Palla et al., (2009,2012). The seepage boundary condition, in which the lower boundary  
534 is set as zero flux when the bottom boundary node is unsaturated and to zero pressure head  
535 when it is saturated, has also been applied to model green roof substrate with Richard's  
536 Equation (Brunetti et al., 2016; Hakimdavar et al., 2014). Model validation presented earlier  
537 has confirmed that the approach adopted in this study provides reasonable predictions of  
538 runoff and vertical water content profile. This section focuses on the influence of these  
539 alternative boundary conditions on the predictions. SWRC B was used for the SWRC and the  
540 Mualem model was adopted to represent the HCF. The lower boundary was set to be free  
541 drainage (Eq. 14) or seepage, and the runoff and the vertical water content profiles were  
542 regenerated for the event of 21/Oct/2013.

$$543 \quad \frac{\partial h}{\partial z} = 0 \quad (14)$$

544 Figure 8(a) shows the modelled runoff using free drainage boundary condition. Compared  
545 with the runoff modelled with constant head boundary condition, the free drainage boundary  
546 condition underestimated the second peak runoff by 13.9% and the peak runoff was also  
547 delayed by 5 minutes. The drain down of the runoff responded slower and lasted longer, the  
548  $R_t^2$  also dropped from 0.902 to 0.752. The long drain down curve was also observed in Liu and  
549 Fassman-Beck, (2017) when using a free drainage boundary condition. Figure 8(b) compares  
550 the monitored and modelled water content profile for the event. Following the storm event,  
551 the modelled water content dropped much faster than the monitored data and the modelled  
552 water content fell well below observed field capacity. Allowing the water content to drain  
553 below field capacity leads to an underestimation of water retained in the substrate. In the

554 study of Palla et al. (2009), the same observation was made, using free drainage boundary  
555 condition with Richard's Equation, the model underestimated the water content for most of  
556 the studied storm events. However, compared with the vertical water content modelled with  
557 constant head boundary condition (Fig. 6(b)), the vertical gradient is less significant, and  
558 therefore more similar to the monitored data.

559 The unrealistic drain-down observed here under free drainage conditions suggests that it is  
560 more appropriate to set the lower boundary condition to a constant suction head when  
561 applying Richard's Equation to model the runoff from green roof substrates.

562 **Fig. 8.** Validation of runoff and temporarily stored moisture. (a) Monitored and modelled  
563 runoff; (b) monitored and modelled vertical water content profiles using SWRC B-Mualem  
564 model and free drainage boundary condition.

565 Figure 9(a) presents the modelled runoff using the seepage boundary condition. The timing  
566 of the runoff profile was wrongly estimated by the model using the seepage boundary  
567 condition. The time to start of runoff was delayed about 75 minutes and the time of peak  
568 runoff was also wrongly predicted; 16.17% less runoff was estimated by the model compared  
569 with the constant head option. The  $R_t^2$  also dropped from 0.902 to 0.691. As the seepage  
570 boundary assumes zeros boundary flux when the bottom boundary is unsaturated, no  
571 outflow is generated until the lower boundary becomes saturated, and as a consequence, a  
572 delay in runoff was generated by the model. Figure 9(b) shows the modelled vertical water  
573 content profiles using the seepage boundary condition. More water was modelled to be  
574 stored in the substrate, which resulted in less runoff being generated. The moisture content  
575 at the bottom boundary corresponds to saturated volumetric water content. Following the

576 storm event, the moisture content in the substrate was modelled to be kept at a high level,  
577 which is inconsistent with the observed moisture content data.

578 The wrongly modelled timing of the runoff profile and the very unrealistic vertical water  
579 content profiles produced using the seepage boundary condition indicate that it is  
580 inappropriate to set seepage as the boundary condition when using Richard's Equation to  
581 model the detention effects of the type of green roof used in this study.

582 **Fig. 9.** Validation of runoff and temporarily stored moisture. (a) Monitored and modelled  
583 runoff; (b) monitored and modelled vertical water content profiles using SWRC B-Mualem  
584 model and the seepage boundary condition.

## 585 **5 Conclusions**

586 Monitored moisture content data was used to investigate moisture content changes within a  
587 green roof substrate during storm events. It was found that once the substrate reaches field  
588 capacity, moisture responses at all three depths in an 80 mm green roof substrate occur  
589 simultaneously, rather than as a wetting front moving downwards. The maximum water  
590 holding capacity determined by FLL tests is consistent with field capacity measured in the  
591 field. The water release curve for HLS green roof substrate was characterised and it has been  
592 confirmed that the green roof substrate is more like a dual porosity system and therefore that  
593 the SWRC is better represented by the Durner equation.

594 Both the Richard's Equation and the lumped Reservoir Routing model can provide reasonable  
595 predictions of runoff profiles, and overall temporary storage dynamics. It should be noted  
596 that, whilst the Reservoir Routing model required calibration from observed rainfall-runoff  
597 performance data, the physically-based Richard's Equation only required data based on the

598 measurable physical characteristics of the substrate (i.e. SWRC, HCF and field capacity).  
599 Validated by five storm events, the approach of using Richard's Equation to represent  
600 temporary (detention) moisture storage between field capacity and saturation proposed in  
601 this paper was proved to be capable of regenerating observed runoff profiles.

602 Discrepancies between the measured and modelled (Richard's Equation) vertical depth  
603 profiles indicate further research is required to investigate the green roof substrate's  
604 unsaturated hydraulic conductivity. Sensitivity analysis conducted with the Richard's Equation  
605 suggested that the modelled runoff profile and vertical water content profile is sensitive to  
606 the HCF.

607 The lower boundary condition has a significant impact on predictions of both runoff and  
608 vertical water content profile in the substrate. It is concluded that neither free drainage nor  
609 seepage boundary conditions are suitable boundary conditions to use with Richard's Equation  
610 to model the detention effects of the green roof used in this study. However the constant  
611 suction head boundary condition was found to represent the observed behaviour better.

## 612 **6 Acknowledgements**

613 Zhangjie Peng is supported by the University of Sheffield, Faculty of Engineering Doctoral  
614 Academy Award. The authors would like to thank Dr. Simon De-Ville, Dr. Christian Berretta  
615 and Dr. Simon Poë for their contribution in establishing the monitoring programme.

## 616 **7 References**

617 ASTM, 2015. Standard Test Methods for measurement of hydraulic conductivity of unsaturated  
618 soils, Astm. <https://doi.org/10.1520/D7664>

619 Berretta, C., Poë, S., Stovin, V., 2014. Moisture content behaviour in extensive green roofs  
620 during dry periods: The influence of vegetation and substrate characteristics. *J. Hydrol.*  
621 511, 374–386. <https://doi.org/10.1016/J.JHYDROL.2014.01.036>

622 Brunetti, G., Šimůnek, J., Piro, P., 2016. A Comprehensive Analysis of the Variably Saturated  
623 Hydraulic Behavior of a Green Roof in a Mediterranean Climate. *Vadose Zo. J.* 15, 0.  
624 <https://doi.org/10.2136/vzj2016.04.0032>

625 Castiglia Feitosa, R., Wilkinson, S., 2016. Modelling green roof stormwater response for  
626 different soil depths. *Landsc. Urban Plan.* 153, 170–179.  
627 <https://doi.org/10.1016/J.LANDURBPLAN.2016.05.007>

628 De-Ville, S., Menon, M., Jia, X., Reed, G., Stovin, V., 2017. The impact of green roof ageing on  
629 substrate characteristics and hydrological performance. *J. Hydrol.* 547, 332–344.  
630 <https://doi.org/10.1016/j.jhydrol.2017.02.006>

631 De-Ville, S., Menon, M., Stovin, V., 2018. Temporal variations in the potential hydrological  
632 performance of extensive green roof systems. *J. Hydrol.* 558, 564–578.  
633 <https://doi.org/10.1016/j.jhydrol.2018.01.055>

634 Durner, W., 1994. Hydraulic conductivity estimation for soils with heterogeneous pore  
635 structure. *Water Resour. Res.* 30, 211–223. <https://doi.org/10.1029/93WR02676>

636 Fassman, E., Simcock, R., 2012. Moisture Measurements as Performance Criteria for Extensive  
637 Living Roof Substrates. *J. Environ. Eng.* 138, 841–851.  
638 [https://doi.org/10.1061/\(ASCE\)EE.1943-7870.0000532](https://doi.org/10.1061/(ASCE)EE.1943-7870.0000532)

639 FLL, 2008. FLL (Forschungsgesellschaft Landschaftsentwicklung Landschaftsbau), (2008).  
640 Guidelines for the Planning, Construction and Maintenance of Green Roofing.

641           Forschungsgesellschaft Landschaftsentwicklung Landschaftsbau e. V., Bonn, Germany.  
642           119.

643   Hakimdavar, R., Culligan, P.J., Finazzi, M., Barontini, S., Ranzi, R., 2014. Scale dynamics of  
644           extensive green roofs: Quantifying the effect of drainage area and rainfall characteristics  
645           on observed and modeled green roof hydrologic performance. *Ecol. Eng.* 73, 494–508.  
646           <https://doi.org/10.1016/J.ECOLENG.2014.09.080>

647   Hilten, R.N., Lawrence, T.M., Tollner, E.W., 2008. Modeling stormwater runoff from green  
648           roofs with HYDRUS-1D. *J. Hydrol.* 358, 288–293.  
649           <https://doi.org/10.1016/j.jhydrol.2008.06.010>

650   Kasmin, H., Stovin, V.R., Hathway, E.A., 2010. Towards a generic rainfall-runoff model for  
651           green roofs. *Water Sci. Technol.* 62, 898. <https://doi.org/10.2166/wst.2010.352>

652   Liu, R., Fassman-Beck, E., 2018. Pore Structure and Unsaturated Hydraulic Conductivity of  
653           Engineered Media for Living Roofs and Bioretention Based on Water Retention Data. *J.*  
654           *Hydrol. Eng.* [https://doi.org/10.1061/\(ASCE\)HE.1943-5584.0001621](https://doi.org/10.1061/(ASCE)HE.1943-5584.0001621).

655   Liu, R., Fassman-Beck, E., 2018. Pore Structure and Unsaturated Hydraulic Conductivity of  
656           Engineered Media for Living Roofs and Bioretention Based on Water Retention Data. *J.*  
657           *Hydrol. Eng.* [https://doi.org/10.1061/\(ASCE\)HE.1943-5584.0001621](https://doi.org/10.1061/(ASCE)HE.1943-5584.0001621)

658   Liu, R., Fassman-Beck, E., 2017. Hydrologic response of engineered media in living roofs and  
659           bioretention to large rainfalls: experiments and modeling. *Hydrol. Process.* 31, 556–572.  
660           <https://doi.org/10.1002/hyp.11044>

661   Liu, R., Fassman-Beck, E., 2016. Effect of Composition on Basic Properties of Engineered  
662           Media for Living Roofs and Bioretention. *J. Hydrol. Eng.* 21, 06016002.

663 [https://doi.org/10.1061/\(ASCE\)HE.1943-5584.0001373](https://doi.org/10.1061/(ASCE)HE.1943-5584.0001373).

664 Marshall, T.J., Holmes, J.W., Rose, C.W., 1996. Soil Physics. Cambridge University Press.

665 <https://doi.org/10.1017/CBO9781139170673>

666 Mualem, Y., 1976. A new model for predicting the hydraulic conductivity of unsaturated

667 porous media. Water Resour. Res. 12, 513–522.

668 <https://doi.org/10.1029/WR012i003p00513>

669 Palla, A., Gnecco, I., Lanza, L.G., 2012. Compared performance of a conceptual and a

670 mechanistic hydrologic models of a green roof. Hydrol. Process. 26, 73–84.

671 <https://doi.org/10.1002/hyp.8112>

672 Palla, A., Gnecco, I., Lanza, L.G., 2009. Unsaturated 2D modelling of subsurface water flow in

673 the coarse-grained porous matrix of a green roof. J. Hydrol. 379, 193–204.

674 <https://doi.org/10.1016/j.jhydrol.2009.10.008>

675 Peng, Z., Stovin, V., 2017. Independent Validation of the SWMM Green Roof Module. J.

676 Hydrol. Eng. 22, 1–12. [https://doi.org/10.1061/\(ASCE\)HE.1943-5584.0001558](https://doi.org/10.1061/(ASCE)HE.1943-5584.0001558).

677 Poë, S., Stovin, V., Berretta, C., 2015. Parameters influencing the regeneration of a green

678 roof's retention capacity via evapotranspiration. J. Hydrol. 523, 356–367.

679 <https://doi.org/10.1016/J.JHYDROL.2015.02.002>

680 Seki, K., 2010. SWRC fit: a nonlinear fitting program with a water retention curve for soils

681 having unimodal and bimodal pore structure. Hydrol. Earth Syst. Sci. Discuss. 4, 407–437.

682 <https://doi.org/10.5194/hessd-4-407-2007>

683 Soulis, K.X., Valiantzas, J.D., Ntoulas, N., Kargas, G., Nektarios, P.A., 2017. Simulation of green

684 roof runoff under different substrate depths and vegetation covers by coupling a simple

685 conceptual and a physically based hydrological model. *J. Environ. Manage.* 200, 434–445.  
686 <https://doi.org/10.1016/j.jenvman.2017.06.012>

687 Stovin, V., Poë, S., De-Ville, S., Berretta, C., 2015. The influence of substrate and vegetation  
688 configuration on green roof hydrological performance. *Ecol. Eng.* 85, 159–172.  
689 <https://doi.org/10.1016/j.ecoleng.2015.09.076>

690 Stovin, V., Vesuviano, G., De-Ville, S., 2017. Defining green roof detention performance.  
691 *Urban Water J.* 14, 574–588. <https://doi.org/10.1080/1573062X.2015.1049279>

692 Stovin, V., Vesuviano, G., Kasmin, H., 2012. The hydrological performance of a green roof test  
693 bed under UK climatic conditions. *J. Hydrol.* 414–415, 148–161.  
694 <https://doi.org/10.1016/J.JHYDROL.2011.10.022>

695 van Genuchten, M.T., 1980. A Closed-form Equation for Predicting the Hydraulic Conductivity  
696 of Unsaturated Soils<sup>1</sup>. *Soil Sci. Soc. Am. J.* 44, 892.  
697 <https://doi.org/10.2136/sssaj1980.03615995004400050002x>

698 Vesuviano, G., Sonnenwald, F., Stovin, V., 2014. A two-stage storage routing model for green  
699 roof runoff detention. *Water Sci. Technol.* 69, 1191.  
700 <https://doi.org/10.2166/wst.2013.808>

701 Vesuviano, G., Stovin, V., 2013. A generic hydrological model for a green roof drainage layer.  
702 *Water Sci. Technol.* 68, 769. <https://doi.org/10.2166/wst.2013.294>

703 Voyde, E., Fassman, E., Simcock, R., Wells, J., 2010. Quantifying Evapotranspiration Rates for  
704 New Zealand Green Roofs. *J. Hydrol. Eng.* 15, 395–403.  
705 [https://doi.org/10.1061/\(ASCE\)HE.1943-5584.0000141](https://doi.org/10.1061/(ASCE)HE.1943-5584.0000141)

706 Yio, M.H.N., Stovin, V., Werdin, J., Vesuviano, G., 2013. Experimental analysis of green roof

707 substrate detention characteristics. *Water Sci. Technol.* 68, 1477–1486.

708 <https://doi.org/10.2166/wst.2013.381>

709 Young, P., Jakeman, A., McMurtrie, R., 1980. An instrumental variable method for model

710 order identification. *Automatica* 16, 281–294. <https://doi.org/10.1016/0005->

711 [1098\(80\)90037-0](https://doi.org/10.1016/0005-1098(80)90037-0)

712

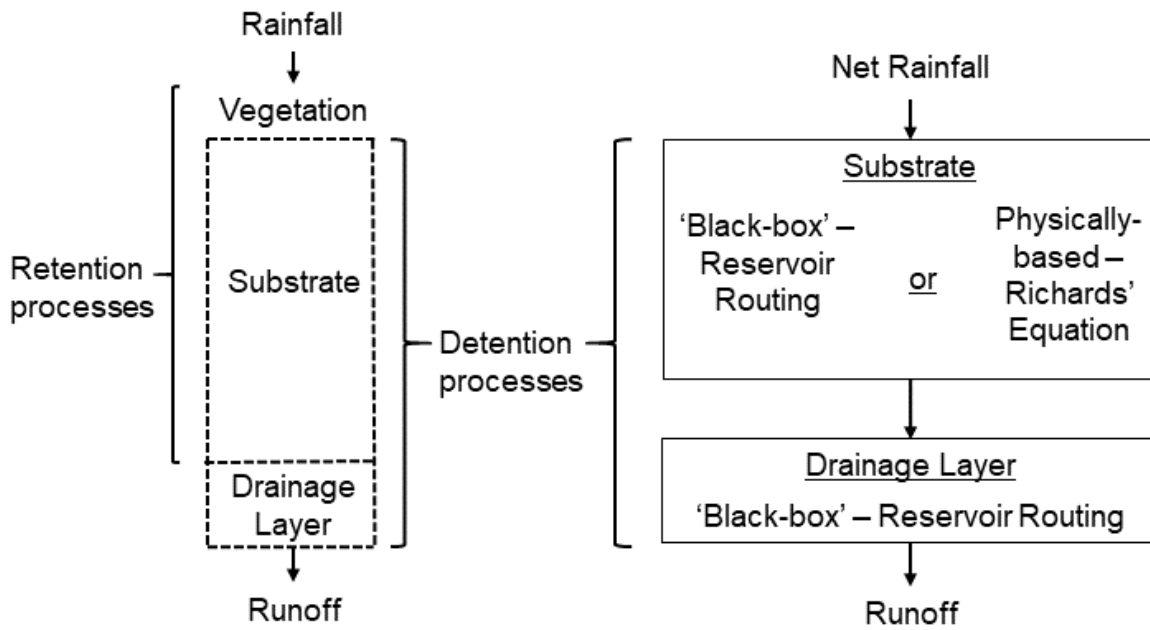


**Fig. 1.** Conceptual green roof hydrological model: left – vertical profile through a typical green roof system indicating the layers associated with retention and detention processes; right – components of a two-stage detention model, indicating the two alternative options for representing substrate detention considered in the present paper.

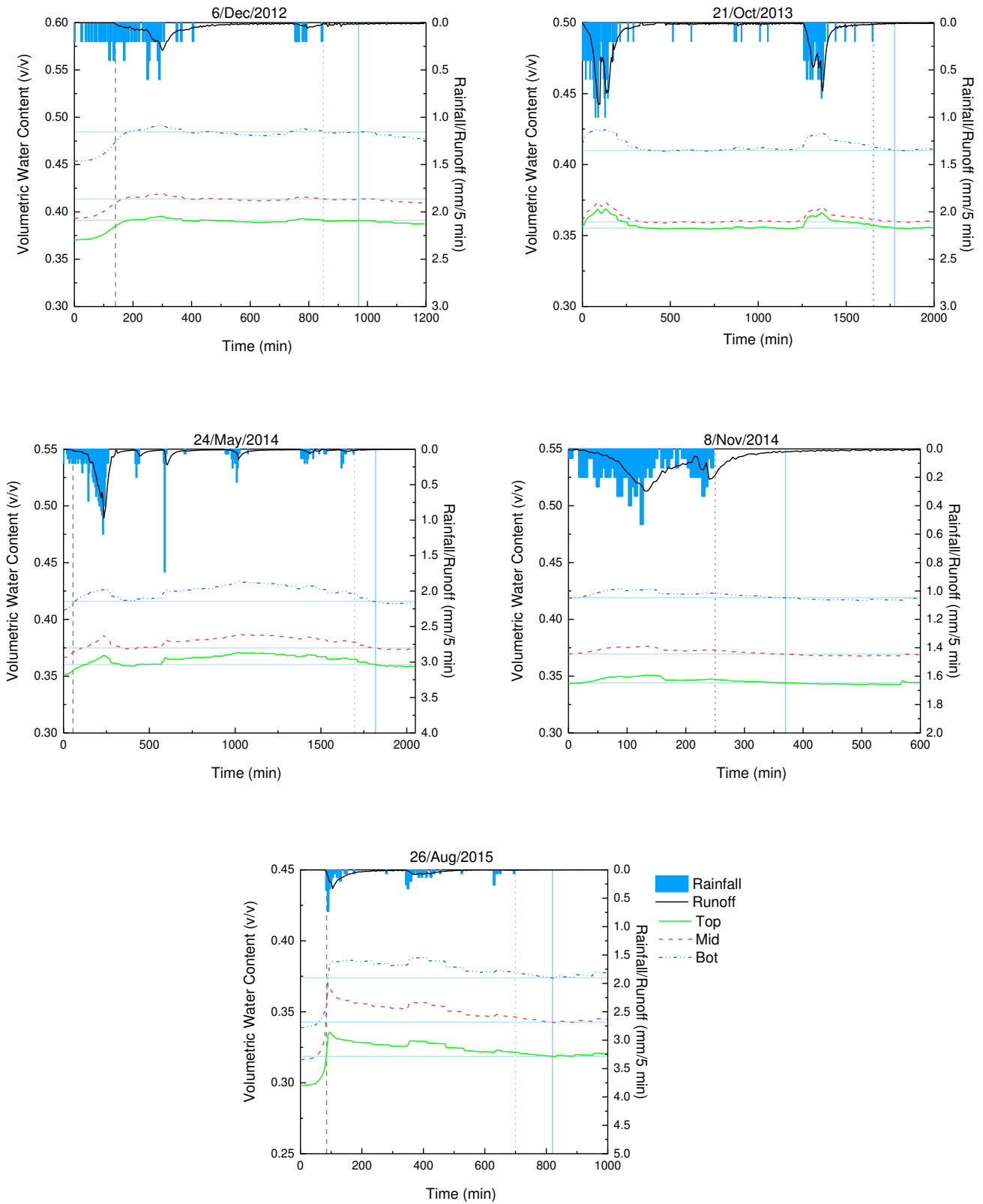
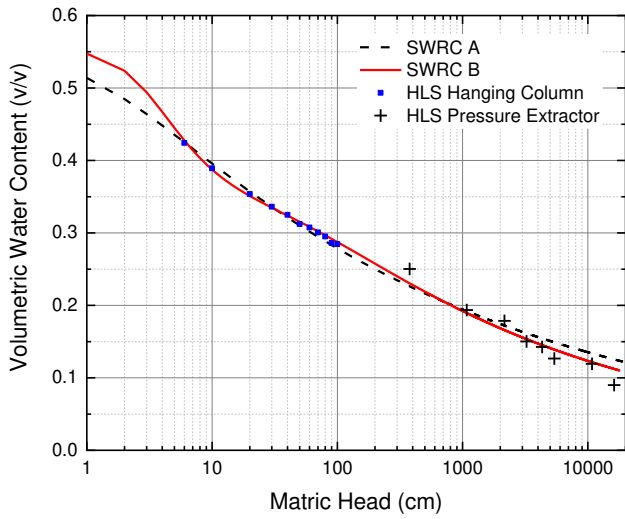
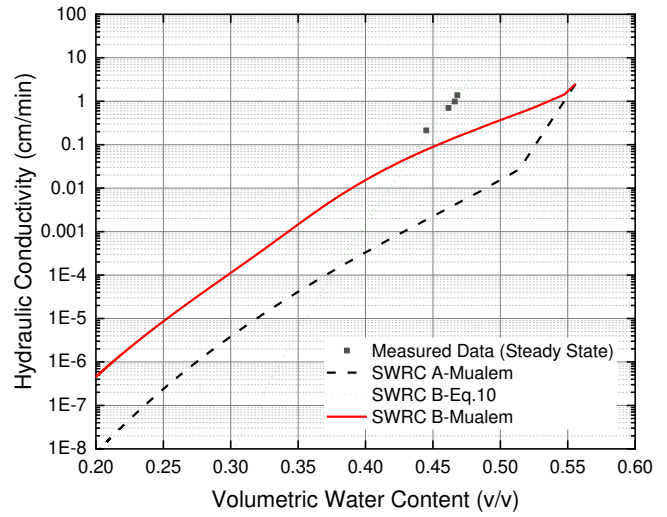


**Fig. 2.** Monitored rainfall, runoff and moisture content profiles for the five selected storm events (vertical dashed line indicates the time significant runoff was firstly observed, dotted line represents the time rainfall stops, the solid vertical line is the time two hours after rainfall stops and the corresponding volumetric water content is assumed to indicate local field capacity).



(a)



(b)

**Fig. 3.** Water release curves and hydraulic conductivity functions. (a) SWRC A is fitted by the Van-Genuchten model, SWRC B is fitted by the Durner model, both models were fitted using hanging column and pressure plate extractor data; (b) plots of the new HCF and the HCFs derived from the two SWRC in (a) via the Mualem model.

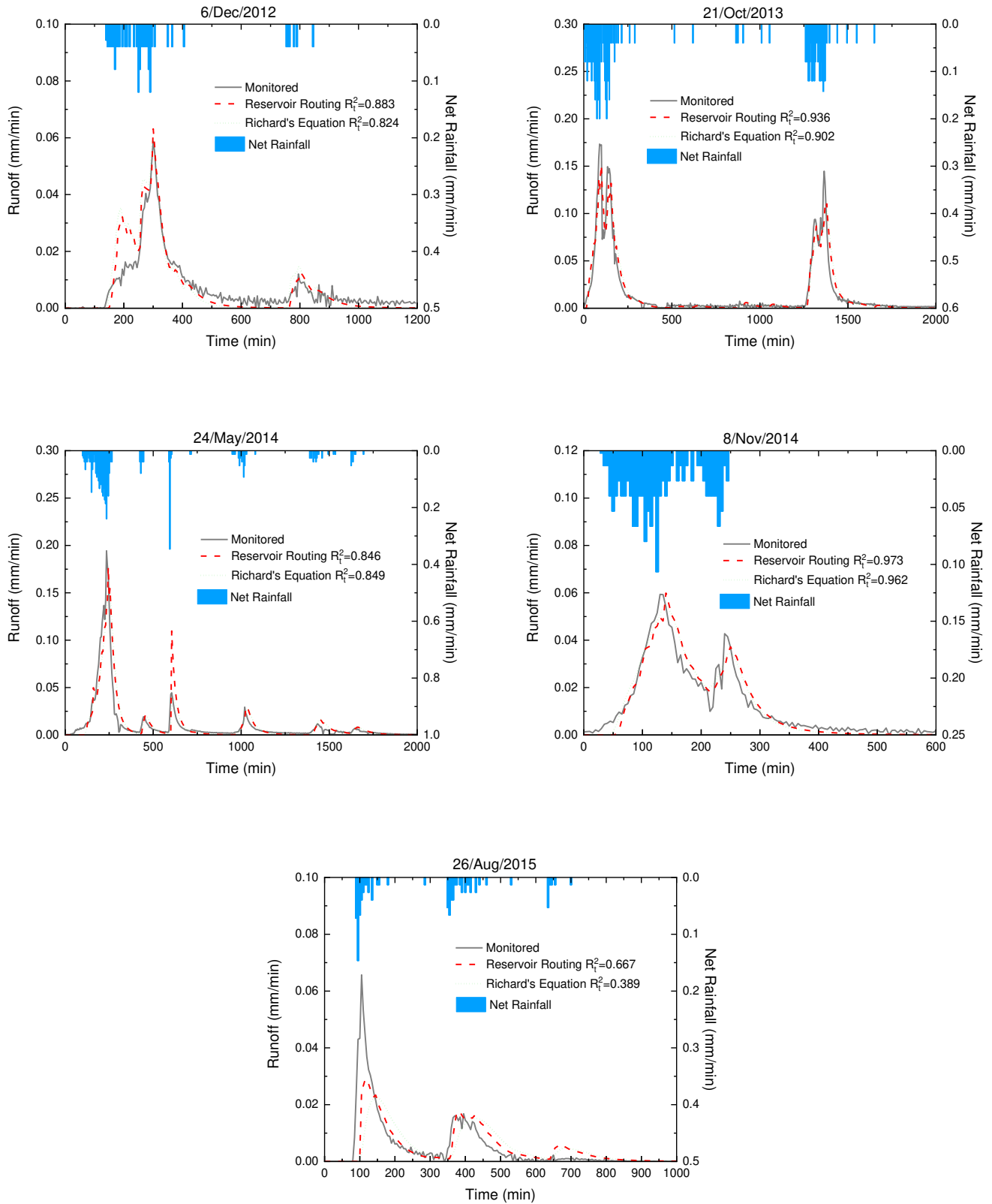
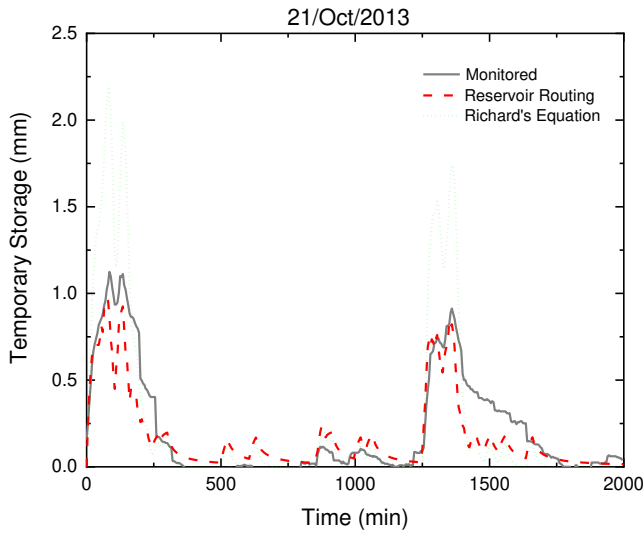
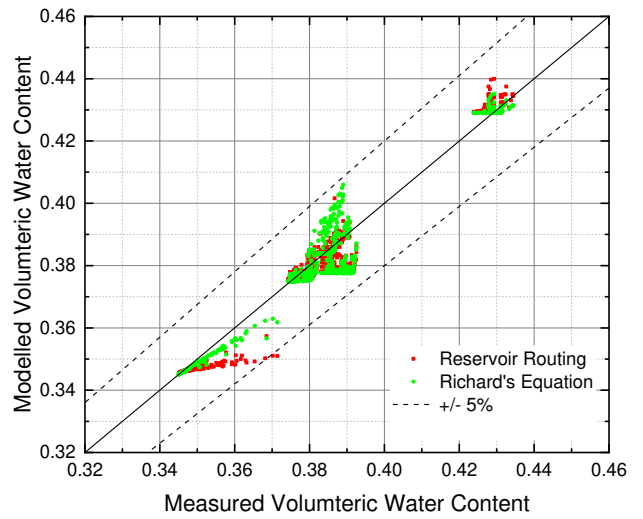


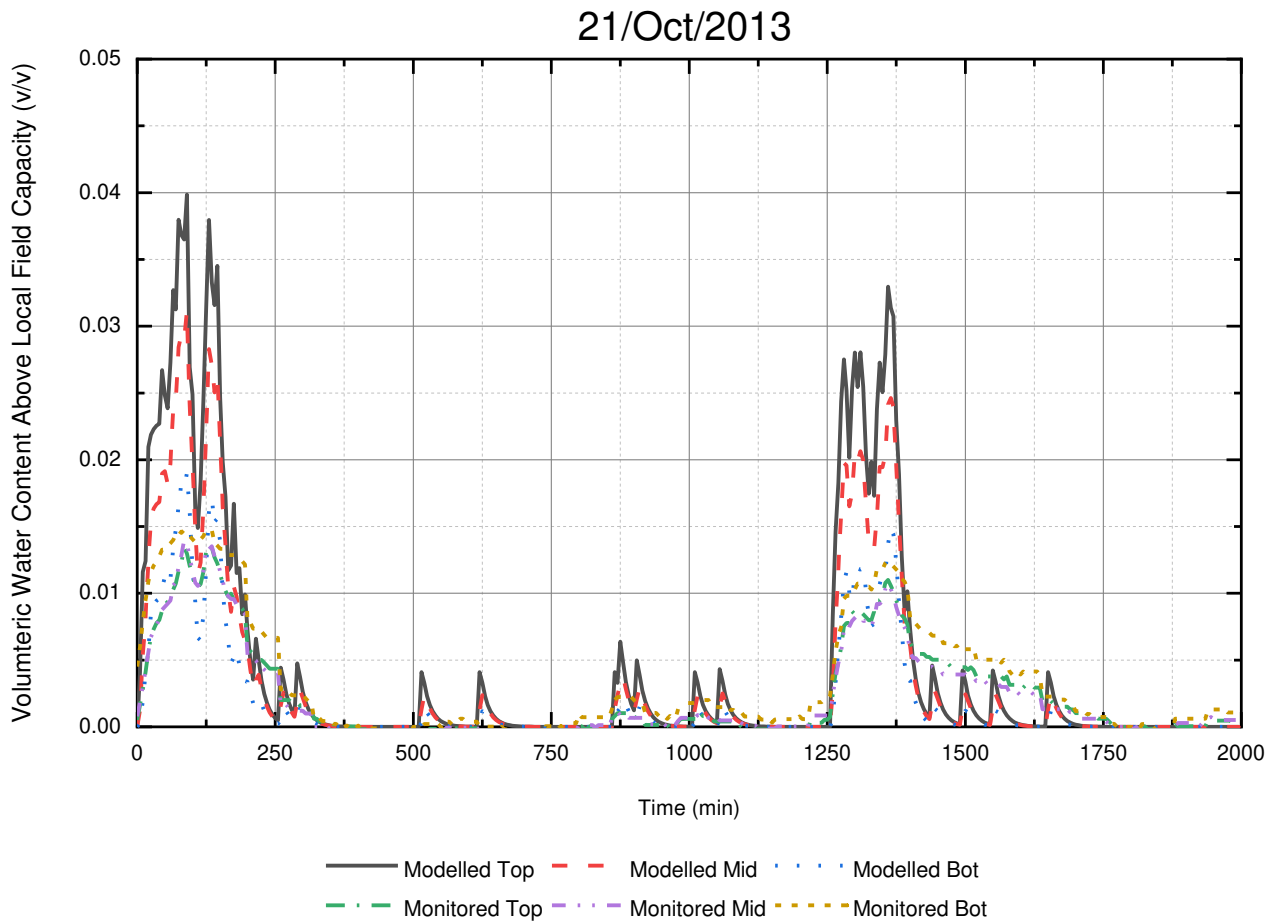
**Fig. 4.** Monitored and modelled runoff using the Reservoir Routing model and the Richard's Equation (Richard's Equation was implemented in MATLAB using SWRC B-Mualem model and constant suction head boundary condition).



(a)

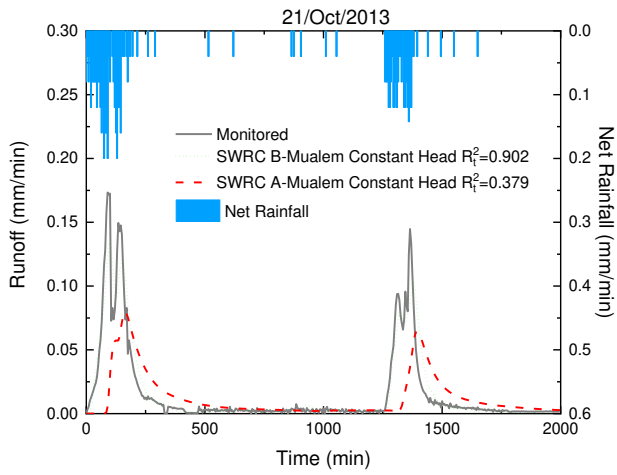


(b)

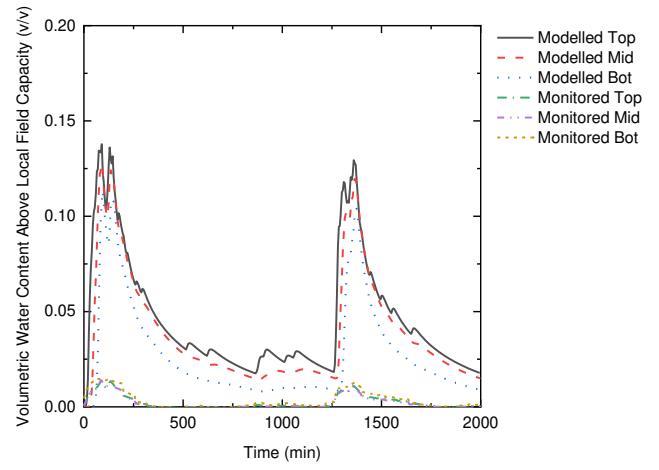


(c)

**Fig. 5.** Validation of temporarily stored moisture. (a) depth averaged temporary storage; (b) scatter plot comparison of water content for all storm events (depth averaged); (c) comparison of vertical water content profiles.

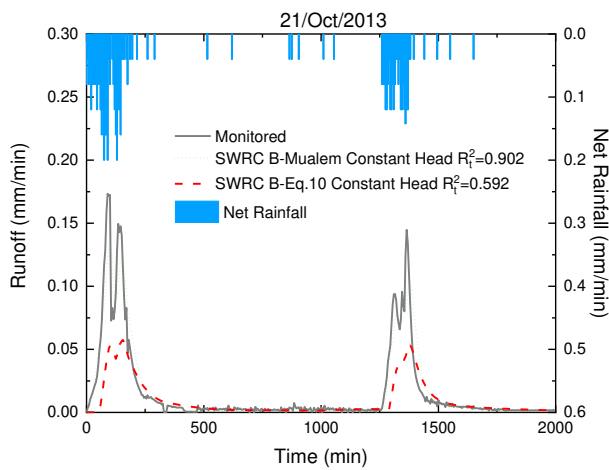


(a)

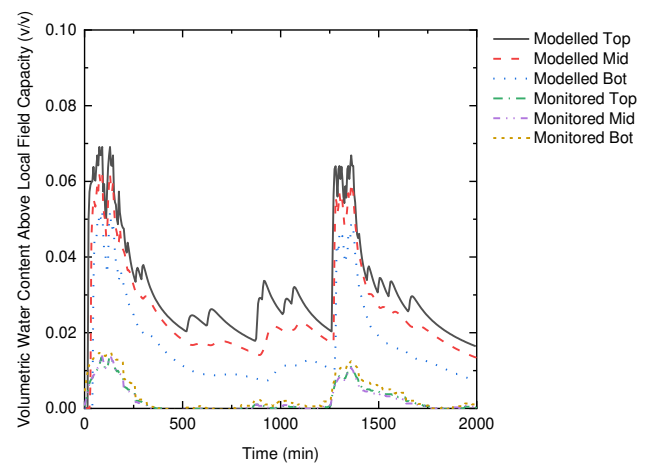


(b)

**Fig. 6.** Validation of runoff and temporarily stored moisture. (a) monitored and modelled runoff; (b) monitored and modelled vertical water content profiles using the SWRC A-Mualem model.



(a)



(b)

**Fig. 7.** Validation of runoff and temporarily stored moisture. (a) monitored and modelled runoff; (b) monitored and modelled vertical water content profiles using SWRC B-Eq. 10 model.

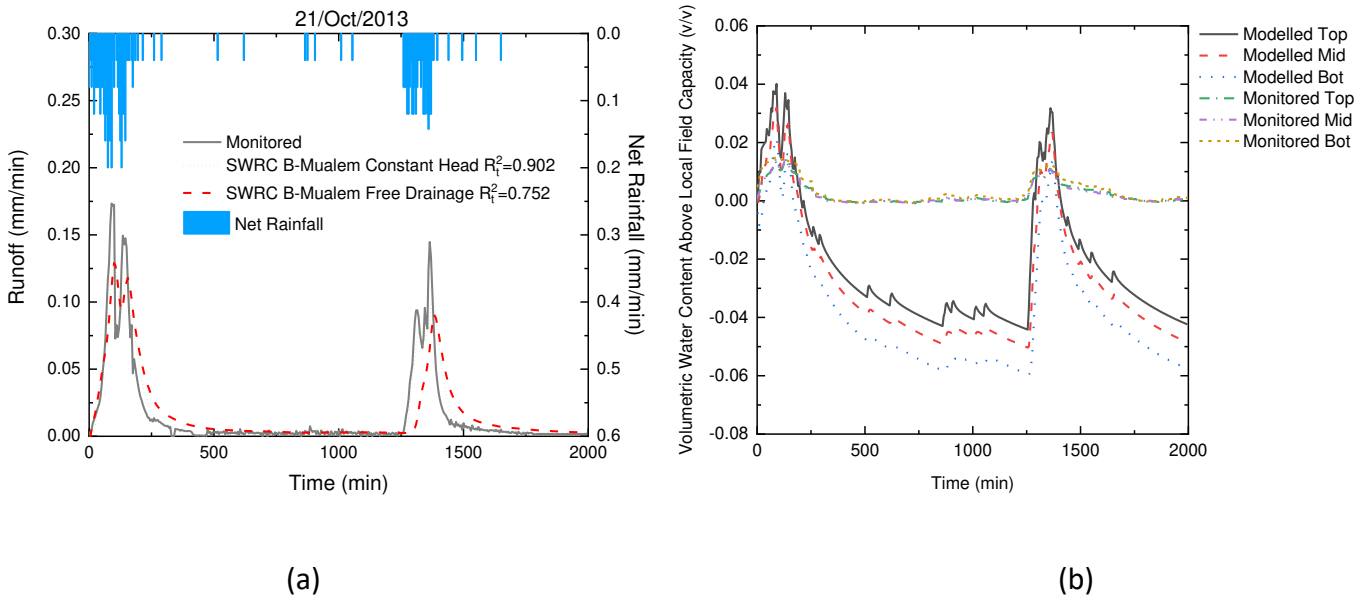


**Fig.8.** Validation of runoff and temporarily stored moisture. (a) Monitored and modelled runoff; (b) monitored and modelled vertical water content profiles using SWRC B-Mualem model and free drainage boundary condition.

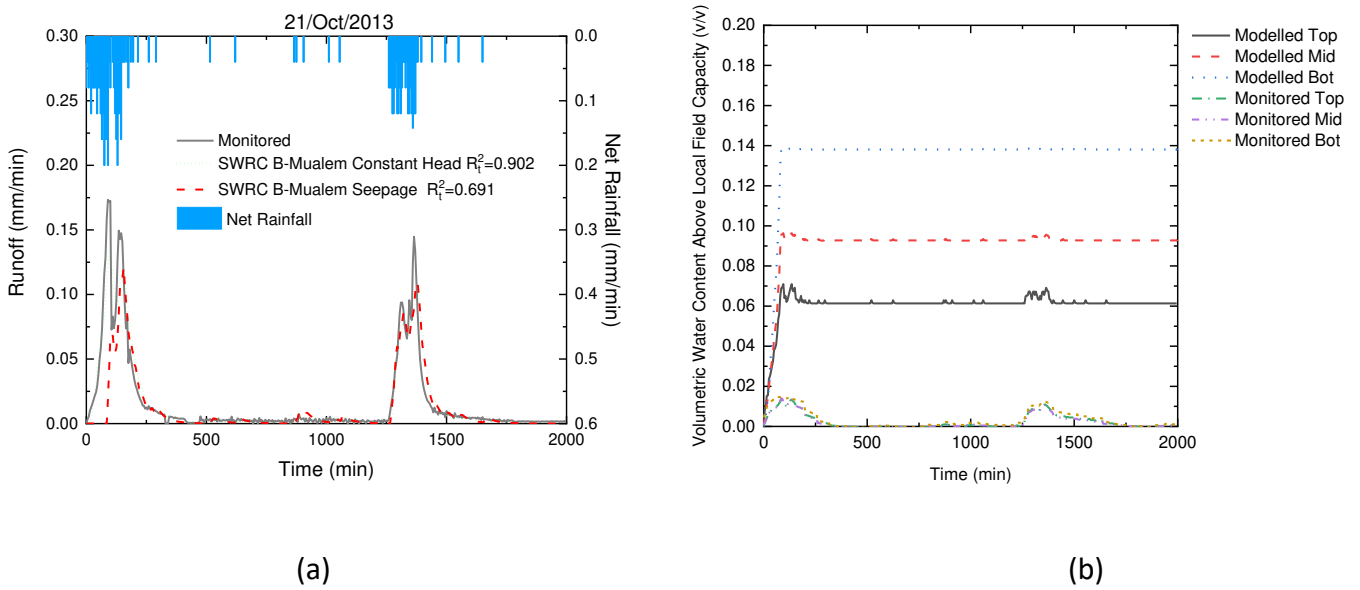


**Fig. 9.** Validation of runoff and temporarily stored moisture. (a) Monitored and modelled runoff; (b) monitored and modelled vertical water content profiles using SWRC B-Mualem model and the seepage boundary condition.

**Table 1.** Value of parameters used in the Reservoir Routing model

Parameter	Value	
	TB7	TB1
$k_g$	0.212	0.175
$n_g$	2.000	2.000
$k_D$	0.026	0.026
$n_D$	1.196	1.196

**Table 2.** Hydrological characteristics of the five selected storm events and TB1 hydrological performance

Event No.	Date	Rainfall Duration (h)	Rainfall depth (mm)	ADWP (h)	Peak rainfall intensity (mm/5 min)	Return Period (yr)	Retention (%)	Initial water content			
								Top	Mid	Bot	Mean
228	06/Dec/2012	14.02	12.20	70.43	0.60	<1	29.97	0.37	0.393	0.453	0.406
292	21/Oct/2013	27.35	31.80	10.90	1.00	>1	0	0.356	0.36	0.414	0.377
361	24/May/2014	28.22	24.13	16.63	1.73	<1	8.73	0.351	0.366	0.408	0.375
396	08/Nov/2014	4.43	8.40	15.52	0.36	<1	6.21	0.344	0.37	0.419	0.377
458	26/Aug/2015	11.63	13.00	57.23	2.67	<1	60.81	0.298	0.316	0.339	0.318

**Table 3.** Local field capacity determined for each storm event

Event No.	Date	Local field capacity			
		TB1			
		Top	Mid	Bot	Mean
228	06/Dec/2012	0.391	0.414	0.485	0.430
292	21/Oct/2013	0.355	0.360	0.410	0.375
361	24/May/2014	0.360	0.375	0.416	0.384
396	08/Nov/2014	0.344	0.396	0.419	0.387
458	26/Aug/2015	0.319	0.343	0.374	0.345
Overall mean					0.384

**Table 4.** HLS Substrate characteristics according to FLL (2008) test methods

Properties	Unit	Mean	St.Dev
Particle size <0.063 mm	%	2.72	0.25
$d_{50}$	mm	5.05	0.07
Bulk density	g/cm <sup>3</sup>	0.81	0.05
Porosity	%	58.10	0.85
Maximum water holding capacity	%	38.53	0.60
Permeability	mm/min	25	7.16

**Table 5.** Fitted parameters for the water release curves for the HLS substrate

Van-Genuchten (SWRC A)		Durner (SWRC B)	
Parameter	Value	Parameter	Value
$\Theta_s$	0.556	$\Theta_s$	0.556
$\Theta_r$	0	$\Theta_r$	0
$\alpha$	0.807	$\alpha_1$	0.306
$n$	1.157	$n_1$	2.255
		$\alpha_2$	0.02
		$n_2$	1.194
		$w_1$	0.378
$R^2$	0.995	$R^2$	0.988